Pflugers Arch - Eur J Physiol
DOI 10.1007/s00424-016-1932-4

SIGNALING AND CELL PHYSIOLOGY

Calcium-gated K^+ channels of the $K_{Ca}1.1$- and $K_{Ca}3.1$-type couple intracellular Ca^{2+} signals to membrane hyperpolarization in mesenchymal stromal cells from the human adipose tissue

Michail V. Tarasov[1] · Marina F. Bystrova[1] · Polina D. Kotova[1] · Olga A. Rogachevskaja[1] · Veronika Y. Sysoeva[2] · Stanislav S. Kolesnikov[1]

Received: 13 September 2016 / Revised: 10 December 2016 / Accepted: 14 December 2016

Abstract Electrogenesis in mesenchymal stromal cells (MSCs) remains poorly understood. Little is known about ion channels active in resting MSCs and activated upon MSC stimulation, particularly, by agonists mobilizing Ca^{2+} in the MSC cytoplasm. A variety of Ca^{2+}-gated ion channels may couple Ca^{2+} signals to polarization of the plasma membrane. Here, we studied MSCs from the human adipose tissue and found that in cells responsive to ATP and adenosine with Ca^{2+} transients or exhibiting spontaneous Ca^{2+} oscillations, Ca^{2+} bursts were associated with hyperpolarization mediated by Ca^{2+}-gated K^+ channels. The expression analysis revealed transcripts for KCNMA1 and KCNN4 genes encoding for Ca^{2+}-activated K^+ channels of large ($K_{Ca}1.1$) and intermediate ($K_{Ca}3.1$) conductance, respectively. Moreover, transcripts for the Ca^{2+}-gated cation channel TRPM4 and anion channels Ano1, Ano2, and bestrophin-1, bestrophin-3, and bestrophin-4 were revealed. In all assayed MSCs, a rise in cytosolic Ca^{2+} stimulated K^+ currents that were inhibited with iberiotoxin. This suggested that $K_{Ca}1.1$ channels are invariably expressed in MSCs. In ATP- and adenosine-responsive cells, iberiotoxin and TRAM-34 diminished electrical responses, implicating both $K_{Ca}1.1$ and $K_{Ca}3.1$ channels in coupling agonist-dependent Ca^{2+} signals to membrane voltage. Functional tests pointed at the existence of two separate MSC subpopulations exhibiting Ca^{2+}-gated anion currents that were mediated by Ano2-like and bestrophin-like anion channels, respectively. Evidence for detectable activity of Ano1 and TRPM4 was not obtained. Thus, $K_{Ca}1.1$ channels are likely to represent the dominant type of Ca^{2+}-activated K^+ channels in MSCs, which can serve in concert with $K_{Ca}3.1$ channels as effectors downstream of G-protein-coupled receptor (GPCR)-mediated Ca^{2+} signaling.

Keywords Mesenchymal stromal cells · Ca^{2+}-activated K^+ channels · Patch clamp · Ca^{2+} imaging · ATP · Adenosine

Introduction

Mesenchymal stromal cells (MSCs) are defined as a heterogeneous cell population that includes adult multipotent cells capable of giving rise to differentiated cells of mesenchymal lines, such as osteoblasts, adipocytes, and chondrocytes [17, 30, 39]. First identified and isolated from the bone marrow, MSCs can now be obtained from a variety of other tissues, including the adipose tissue, umbilical cord blood, skin, and some others [6, 25, 33]. Although it is widely accepted that MSCs are crucial to tissue regeneration, molecular mechanisms controlling proliferation, migration, secretion, and differentiation of individual cells are still poorly understood.

Intracellular Ca^{2+} is a highly versatile second messenger involved in the regulation of almost all cellular functions [14, 49]. Particularly, spontaneous Ca^{2+} oscillations and Ca^{2+} transients evoked by local environmental cues can govern gene expression, cell proliferation and differentiation, and expansion of progenitor pools [2, 7, 31]. Thus, membrane receptors and signaling pathways associated with intracellular Ca^{2+} signaling may be critically important for the maintenance

Electronic supplementary material The online version of this article (doi:10.1007/s00424-016-1932-4) contains supplementary material, which is available to authorized users.

✉ Stanislav S. Kolesnikov
staskolesnikov@yahoo.com

[1] Institute of Cell Biophysics, Russian Academy of Sciences, Institutional Street 3, Pushchino, Moscow Region, Russia 142290

[2] Department of Biochemistry and Molecular Medicine, Faculty of Basic Medicine, Lomonosov Moscow State University, Moscow, Russia

Published online: 27 December 2016

of a MSC population as well as for the regulation of MSC migration and differentiation.

Although the main function of ion channels is to control ion fluxes through the plasma membrane, they also can play a much less appreciated role in coordinating extracellular and intracellular signals associated with cell proliferation and differentiation [3, 5, 48, 57]. Ion channels can regulate exocytosis of autocrine and paracrine factors by setting Ca^{2+} influx directly or determining one indirectly via membrane potential [3, 7]. Ion channels are also capable of modulating cell proliferation and differentiation via flux-independent mechanisms, including association of channel proteins with membrane receptors [13, 66]. As a specific example, the Ca^{2+}-activated cation channel TRPM4 is involved in differentiation of dental follicle stem cells, playing an inhibitory role in osteogenesis but being required for differentiation into adipocytes [42]. TRPM7 activity is required for bone marrow stem cell proliferation and viability [11]. The delayed rectifier K^+ channels and Ca^{2+}-activated K^+ channels are required for MSC proliferation [16, 64]. Vascular smooth muscle cell proliferation critically depends on activity of large conductance Ca^{2+}-gated K^+ channel ($K_{Ca}1.1$ channels) [29].

As we found recently, the population of MSCs derived from the human adipose tissue is functionally heterogeneous in that it contains multiple subpopulation, each being specifically responsive to a particular agonist of G-protein-coupled receptors (GPCR), such as ATP, adenosine, noradrenalin, and some others [35]. These substances elicited Ca^{2+} transients in resting MSCs but weakly affected spontaneous Ca^{2+} oscillations observed in a small fraction of non-stimulated cells. Physiological significance of the agonist-dependent Ca^{2+} mobilization in MSCs and their oscillatory behavior remain largely unknown. Extracellular ATP, its downstream product adenosine, and related nucleotides are ubiquitous signaling molecules, operating in virtually all tissues and cells. In particular, MSCs are endowed with several purinergic receptors and ectonucleotidases and release extracellular purines presumably to mediate/promote growth/proliferation, pro- or anti-apoptotic processes, differentiation, and immunomodulation [52]. Here, we consider the immediate consequence of intracellular Ca^{2+} bursting, that is a Ca^{2+}-dependent change in ion channel activity and provides evidence that in MSCs, Ca^{2+} signaling is associated with cell hyperpolarization that is largely mediated by Ca^{2+}-gated K^+ channels of the $K_{Ca}1.1$ and $K_{Ca}3.1$ types.

Materials and methods

MSC isolation and culturing

Human MSCs were isolated from the subcutaneous adipose tissue of 15 healthy (i.e., without infectious, systemic diseases or malignancies) men from 32 to 60 years old. The body mass index (BMI) of individuals varied from 20 to 29. No clear correlation between BMI and physiological features of MSCs was found. All donors gave informed consent for harvesting their adipose tissue.

Isolation and characterization of cells were described earlier [35]. Briefly, the adipose tissue was extensively washed with two volumes of Hank's Balanced Salt Solution (HBSS) containing 5% antibiotic/antimycotic solution (HyClone), fragmented and then digested at 37 °C for 1 h in the presence of collagenase (200 U/ml, Sigma-Aldrich) and dispase (10 U/ml, BD Biosciences). Enzymatic activity was neutralized by adding an equal volume of a culture medium (Advance Stem basal medium for human undifferentiated mesenchymal stem cells (HyClone)) containing 10% of Advance stem cell growth supplement (CGS) (HyClone) and 1% antibiotic/antimycotic solution and centrifuged at 200 g for 10 min. This led to the sedimentation of diverse cells, including MSCs, macrophages, lymphocytes, and erythrocytes, unlike adipocytes that remained floating. After removal of supernatant, a lysis solution (154 mM NH_4Cl, 10 mM $KHCO_3$, and 0.1 mM EDTA) was added to a cell pellet to lyse erythrocytes, and cell suspension was centrifuged at 200 g for 10 min. Sedimented cells were resuspended in the MSC culture medium and filtered through a 100 μm nylon cell strainer (BD Biosciences). As indicated by flow cytometry [35], after isolation and overnight pre-plating, the obtained cell population contained not only MSC cells that basically represented the most abundant subgroup but also admixed macrophages and lymphocytes. The two last cell subgroups were dramatically depleted by culturing for a week in the MSC culture medium and humidified atmosphere (5% CO_2) at 37 °C. The obtained MSC population was maintained at a subconfluent level (~80% confluency) and passaged using HyQTase (HyClone). For experiments, cells of the second to fourth passages were used.

Preparation of cells for patch clamping and Ca^{2+} imaging

Prior to physiological experiments, cells were maintained in a 12 socket plate for 12 h in the medium described above but without antibiotics. For isolation, cells cultured in a 1 ml socket were rinsed twice with the Versen solution (Sigma-Aldrich) that was then substituted for 0.2 ml HyQTase solution (HyClone) for 3–5 min. The enzymatic treatment was terminated by the addition of 0.8 ml culture medium to a socket. Next, cells were resuspended, and cell suspension was put into a tube for storage in the MSC culture medium at 4 °C for 6–8 h. When necessary, isolated cells were collected by a plastic pipette and plated onto a recording chamber. After sedimentation and attachment to the chamber bottom coated with the Cell-Tak adhesive (BD Biosciences), cells were loaded with Fluo-4 at room temperature (23–25 °C) by adding Fluo-4AM (4 μM) and Pluronic (0,02%) (all from Molecular Probes) to the bath solution (mM): 135 NaCl, 5 KCl, 1 $MgCl_2$, 2 $CaCl_2$, and 10

HEPES-NaOH (NaOH), pH 7.4. After the 20-min incubation, cells were rinsed several times with the bath solution.

Electrophysiology

Electrophysiological activity of MSCs was assayed with the patch clamp technique under the whole-cell (WC) mode or using the perforated patch approach. Ion currents were recorded, filtered, and analyzed using an Axopatch 200B amplifier, Digidata 1332A and MiniDigi 1A interfaces, and the pCLAMP 8 software (all from Molecular Devices). Cells were polarized either by serial voltage pulses of appropriate duration at a 10–20 mV step or by voltage ramp (1 mV/ms). The basic intracellular solution contained (mM) 140 KCl (CsCl), 1 $MgCl_2$, 0.1 EGTA, and 10 HEPES-KOH (KOH), pH 7.3. In certain cases, cells were dialyzed with the solution containing 440 nM free Ca^{2+} (mM): 140 CsCl, 1 $MgCl_2$, 7.9 $CaCl_2$ + 10 EGTA-CsOH, 10 HEPES-CsOH, and 2 ATP-Mg, pH 7.3. For WC or perforated patch recordings, 2 mM MgATP or amphotericin B (400 μg/ml) was added into the intracellular solution, respectively. The basic extracellular solution contained (mM) 135 NaCl, 5 KCl, 1 $MgCl_2$, 2 $CaCl_2$, and 10 HEPES-NaOH (NaOH), pH 7.4. When required, it was modified in that NaCl was replaced with Na-HEPES (low Cl^- solution). The recording chamber of nearly 75 μl and gravity-driven perfusion system have been described previously [34]. All chemicals were bath applied for 1 s and rinsed within 3 s. Buffers, salts, ATP, and adenosine were from Sigma-Aldrich; apamin, iberiotoxin, TRAM-34, CaCCinh-A01, and T16Ainh-A01 were from Tocris. Experiments were carried out at room temperature (22–24 °C).

Imaging

Cells loaded with Fluo-4 were imaged by using a fluorescent microscope Axioscope 2 equipped with an objective Plan-Neofluar 20×/0.50 (Zeiss) and ECCD camera LucaR (Andor Technology). Apart from a transparent light illuminator, the microscope was equipped with a handmade system for epi-illumination via an objective. Fluo-4 fluorescence was excited by using a computer-controllable light emitting diode (LED) LZ1-00B700H (Ledengin). LED emission was filtered with an optical filter ET480/20× (Chroma Technology). Fluo-4 emission was collected at 535 ± 25 nM by using emission filter ET535/50m (Chroma Technology). Serial fluorescent images were captured every second and analyzed with the Imaging Workbench 6 software (INDEC). The deviation of cytosolic Ca^{2+} from the resting level in an individual cell was quantified by the relative change in Fluo-4 fluorescence $\Delta F/F_0$, where $\Delta F = F - F_0$; F is the instant intensity of cell fluorescence and F_0 is the intensity of cell fluorescence obtained in the very beginning of a recording and averaged over a 20-s interval. In certain cases, cells preloaded with Fluo-4 were patch clamped, and their electrophysiological characteristics were analyzed simultaneously with intracellular Ca^{2+} monitoring.

RT-PCR

Total RNA was extracted from a sample containing 10^5–10^6 MSCs by using the RNeasy Mini Kit (Qiagen). Isolated RNA was treated with DNase I (Ambion) and reverse transcribed with PrimeScript reverse transcriptase (TaKaRa) and random hexamer primers, following the manufacturer's instruction. Obtained cDNA served as a template for PCR with gene-specific primers that were designed to recognize sequences of all known splice variants of human genes encoding Ca^{2+}-gated K^+ channels, bestrophins, and anoctanins as well as three marker genes for MSCs, including CD73, CD90, and CD105 (Supplementary Materials, Table S1). The expected sizes of PCR products were as follows (in bp): KCNMA1–446, KCNN1–316, KCNN2–445, KCNN3–268, KCNN4–330; CD73–266, CD90–344, CD105–317; TRPM4–367, TRPM5–273; Ano1–295, Ano2–329, Ano3–444, Ano4–311, Ano5–252, Ano6–262, Ano7–321, Ano8–364, Ano9–367, Ano10 and Ano332; Best1–282, Best2–300, Best3–198, Best4–316. The PCR products were verified by direct sequencing (Evrogen, Moscow).

Results

In order to probe functional coupling of Ca^{2+} signals to membrane polarization, a number of MSCs were concurrently assayed with the Ca^{2+} imaging and the patch clamp technique. In designated experiments, we loaded MSCs with Fluo-4 and searched for cells that exhibited spontaneous Ca^{2+} oscillations or were responsive to ATP or adenosine, the purinergic agonists shown to mobilize intracellular Ca^{2+} in MSCs [19, 35, 67]. If generated spontaneous or agonist-induced Ca^{2+} signals, a cell was then examined with the patch clamp technique. It should be noted that patch clamping frequently stopped Ca^{2+} oscillations in wavering cells and also rendered purinergic MSCs irresponsive to ATP and adenosine for a currently undetermined reason. Perhaps, being unavoidable for gigaseal formation, the mechanical disturbance of an assayed cell destroyed intracellular machinery responsible for Ca^{2+} signaling. Because of this interfering phenomenon, most of oscillating and purinergic MSCs could not be effectively assayed with the patch clamp technique and Ca^{2+} imaging in concurrent recordings. Eventually, we succeeded in conclusive recordings from seven MSCs with oscillating cytosolic Ca^{2+} and found that in all of them, membrane voltage varied synchronously with cytosolic Ca^{2+} (Fig. 1a). Given that a rise in cytosolic Ca^{2+} was accompanied by cell hyperpolarization, Ca^{2+}-dependent stimulation of K^+ channels or inhibition of

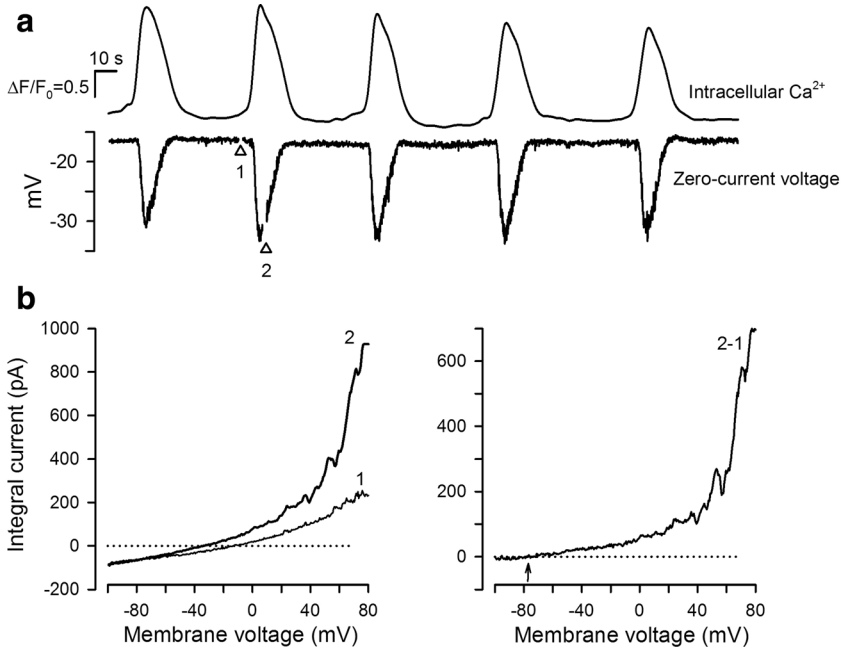

Fig. 1 Oscillations of intracellular Ca^{2+} are associated with a periodic increase in K^+ conductance. **a** Representative example (n = 7) of concurrent monitoring of intracellular Ca^{2+} *(upper panel)* and membrane voltage (*bottom panel*) in MSC loaded with Fluo-4. *Upper panel*, the data are presented as $\Delta F/F_0$, where $\Delta F = F - F_0$; F is the instant intensity of cell fluorescence, and F_0 is the intensity of cell fluorescence obtained in the very beginning of the recording and averaged over a 20-s interval. *Bottom panel*, membrane voltage synchronously recorded under zero-current clamp. The recording was interrupted at the moments *1* and *2* to generate I-V curves under the voltage clamp mode. In this case, an assayed cell was held at −40 mV and polarized by a voltage ramp (1 mV/ms) between −100 and 80 mV. **b** *Left panel*, I-V curves generated at the moments *1* and *2* as indicated in the *bottom panel* in (**a**). *Right panel*, the I-V curve of Ca^{2+}-dependent current determined as a difference of I-V curves 2 and 1 presented in the *left panel*. The current reversed at nearly −80 mV (*arrow*), suggesting Ca^{2+}-activated K^+ channels to be responsible. The perforated patch approach was employed. The patch pipette was filled with 140 mM KCl + 400 μg/ml amphotericin B; the bath solution contains 135 mM NaCl +5 mM KCl

cationic and/or Cl^- channels was obligatory for this phenomenon. To probe into ionic specificity of responsible channels, we generated current-voltage (I-V) curves when Ca^{2+} reached the lowest and maximal levels. Since input resistance varied from cell to cell within an order of magnitude, current injection produced an unpredictable voltage response in a given cell assayed under the current clamp mode. We therefore used the following protocol. Basically executed under zero-current clamp, a recording was switched to voltage clamp for 3–5 s to generate an I-V curve with a voltage ramp (1 mV/ms) polarizing a cell from −100 to 80 mV, and then, the acquisition was returned to the current clamp (Fig. 1a, bottom panel, triangles 1 and 2). The representative I-V curves shown in Fig. 1b (left panel) clearly indicated that a Ca^{2+} transient in the MSC cytoplasm stimulated a marked increase in membrane conductance and shifted a reversal potential of an integral current to the left by 30–40 mV. The Ca^{2+}-dependent current, which was determined as a difference between integral currents measured at minimal and maximal Ca^{2+} (Fig. 1b, right panel), reversed at nearly −78 ± 1.3 mV on average (n = 9). This value is quite close to the Nernst potential for K^+ ions that is equal to −85 mV at the $[140\ mM]_{in}/[5\ mM]_{out}$ gradient and 22 °C. It thus appeared that the periodic hyperpolarization observed in MSCs with spontaneous Ca^{2+} oscillations (Fig. 1a) was mainly associated with stimulation of Ca^{2+}-gated K^+ channels by Ca^{2+} bursts.

Expression of Ca^{2+}-gated ion channels in MSCs

The family of Ca^{2+}-activated K^+ channels is functionally subdivided into small ($K_{Ca}2.x$), intermediate ($K_{Ca}3.1$), and large ($K_{Ca}1.1$) conductance channels [4, 56, 61]. In mammalians, a single gene *KCNMA1* encodes the pore-forming α subunit of $K_{Ca}1.1$ channels [50], three genes, including *KCNN1*, *KCNN2*, and *KCNN3* encode $K_{Ca}2.x$ channels, while *KCNN4* encodes the $K_{Ca}3.1$ channel [56, 65]. By using conventional RT-PCR and gene-specific primers, we analyzed expression of the abovementioned genes in MSCs. It turned out that all RNA preparations (n = 5) isolated from MSC colonies of nearly 10^6 cells contained transcripts for *KCNMA1* and *KCNN4*, while *KCNN1*, *KCNN2*, and *KCNN3* transcripts were undetectable (Fig. 2a). These findings indicated that Ca^{2+}-activated K^+ currents in MSCs (Fig. 1) were presumably mediated by $K_{Ca}1.1$ and/or $K_{Ca}3.1$ channels. Apart from specialized K^+ channels mentioned previously, Ca^{2+} ions also gate the cation channels TRPM4 and TRPM5 [21] as well as anion channels formed by certain channel subunits from the anoctamin (TMEM16) and

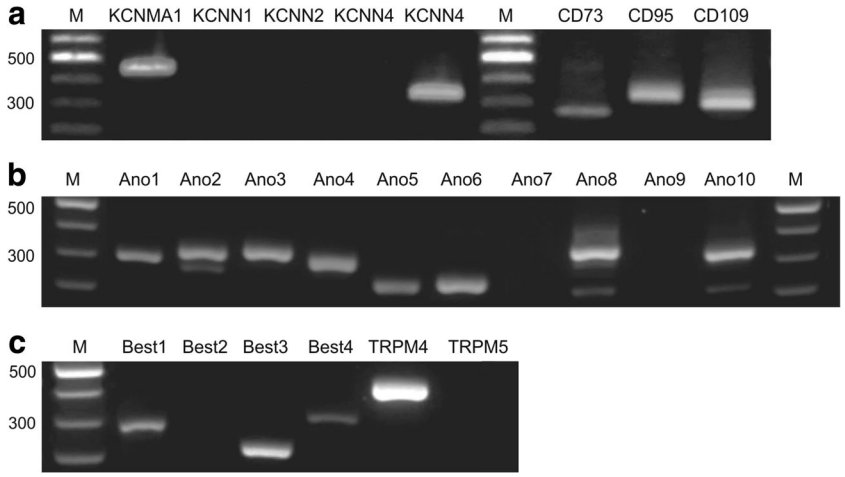

Fig. 2 RT-PCR analysis of expression of Ca^{2+}-gated channels in MSCs. **a** Detected amplicons of expected sizes (bp) correspond to transcripts for the *KCNMA1* (446) and *KNCK4* (330) genes encoding for $K_{Ca}1.1$ and $K_{Ca}3.1$ channels, respectively, as well as for the marker genes *CD73* (266), *CD90* (344), and *CD105* (317). Products of expected sizes for *KCNN1* (316), *KCNN2* (445), and *KCNN3* (268) were not detectable. **b** Detection of transcripts for anoctamins. Fragments of expected sizes were obtained for *Ano1* (295), *Ano2* (329), *Ano3* (444), *Ano4* (311), *Ano5* (252), *Ano6* (262), *Ano8* (364), and *Ano*10 (332). Transcripts for *Ano7* (321) and *Ano9* (367) were undetectable. **c** Detection of transcripts for bestrophins and TRPM channels. Fragments of expected sizes were obtained for Best1 (282), Best4 (316), and TRPM4 (367). In the case of Best3, transcript variant 2 (NM 152439.3) (198) was found, while transcript variants 1, 3, and 4 (351) as well as Best2 (300) and TRPM5 (273) were not detected. The molecular weight markers (M) were GeneRuler 100 bp DNA Ladder (Fermentas). The agarose gels (1.3%) were stained with ethidium bromide. No specific signals were detected in the no RT control

bestrophin families. Among them, Ano1 (TMEM16A), Ano2 (TMEM16B), and Best1 have been reported to form Ca^{2+}-activated anion channels in a variety of cells [37, 53]. These Ca^{2+}-dependent cation and anion channels could also couple intracellular Ca^{2+} signals to plasma membrane polarization. We therefore analyzed their expression in MSCs and detected transcripts for Ano1 and Ano2 and several other anoctamins as well as for bestrophin-1, bestrophin-3, and bestrophin-4 (Fig. 2c, d).

Ion currents regulated by intracellular Ca^{2+} in MSCs

Next, we tried to reveal functional activity of the Ca^{2+}-gated ionic channels that were identified in MSCs at the messenger RNA (mRNA) transcript level (Fig. 2). Note that intracellular Ca^{2+} oscillated spontaneously (Fig. 1a) in a small (3–5%) MSC subpopulation so that the vast majority of assayed cells exhibited relatively stable resting potentials ranging between −10 and −40 mV with 140 mM KCl in the pipette and 135 mM NaCl + 5 mM KCl in the bath. When treated with Ca^{2+} ionophore ionomycin (5 μM), all MSCs assayed in this series (n = 51) were hyperpolarized by 20–40 mV. Iberiotoxin (IbTX) (100 nM), a specific blocker of $K_{Ca}1.1$ channels, reversed the ionomycin effect partly or completely (Fig. 3a). Consistent with activity of $K_{Ca}1.1$ channels, large IbTX-sensitive, outwardly rectifying, voltage-gated currents were seen in cells, wherein ionomycin sufficiently elevated cytosolic Ca^{2+} (Fig. 3b, c). In contrast, ionomycin effects were not reversed by the specific $K_{Ca}3.1$ channel blocker TRAM-34 (1 μM) in most (88%) assayed MSCs (Fig. 3d, e), suggesting negligible contribution of $K_{Ca}3.1$ channels to the ionomycin-induced hyperpolarization of these cells. Nevertheless, among 51 assayed MSCs hyperpolarized by 5 μM ionomycin, six cells (12%) were significantly or almost completely repolarized by 1 μM TRAM-34, while 100 nM IbTX elicited only small additional depolarization (Fig. 3f). In all these cases, TRAM-34 exerted a small decrease in membrane conductance that was detectable at negative voltages but masked at positive potentials by large and nosy outward currents mediated by $K_{Ca}1.1$ channels (Fig. 3g). Together, the abovementioned findings led us to the conclusion that $K_{Ca}1.1$ channels represent the main type of Ca^{2+}-gated K^+ channels that were functional in the vast majority, if not each of MSCs, while ionomycin-induced activity of $K_{Ca}3.1$ channels was characteristic of a small MSC subpopulation.

Because large and noisy currents mediated by $K_{Ca}1.1$ channels greatly complicated reliable identification of Ca^{2+}-dependent anionic and cationic channels, we dialyzed a number of hAD-MSCs with a CsCl-based intracellular solution to completely suppress Ca^{2+}-activated K^+ currents. When perforated patch approach was employed, 5 μM ionomycin elicited marked inward currents in 12 out of 45 cells (27%) held at −60 mV and increased their conductance (Supplementary Materials, Fig. S1). In all cases, ionomycin-induced currents in Cs^+-dialyzed cells were suppressed by the common inhibitor of Ca^{2+}-gated anionic channels CaCCinh-A01 (CaCCinh) (100 μM) (Fig. S1) and several blockers of anionic channels such as SITS (500 μM) and 9-AC (2 mM) (not shown). In contrast, assayed cells were negligibly sensitive to 9-phenanthrol (300 nM) (Fig. S1), a specific TRPM4 blocker [22]. Thus, with CsCl in the pipette and NaCl in the bath,

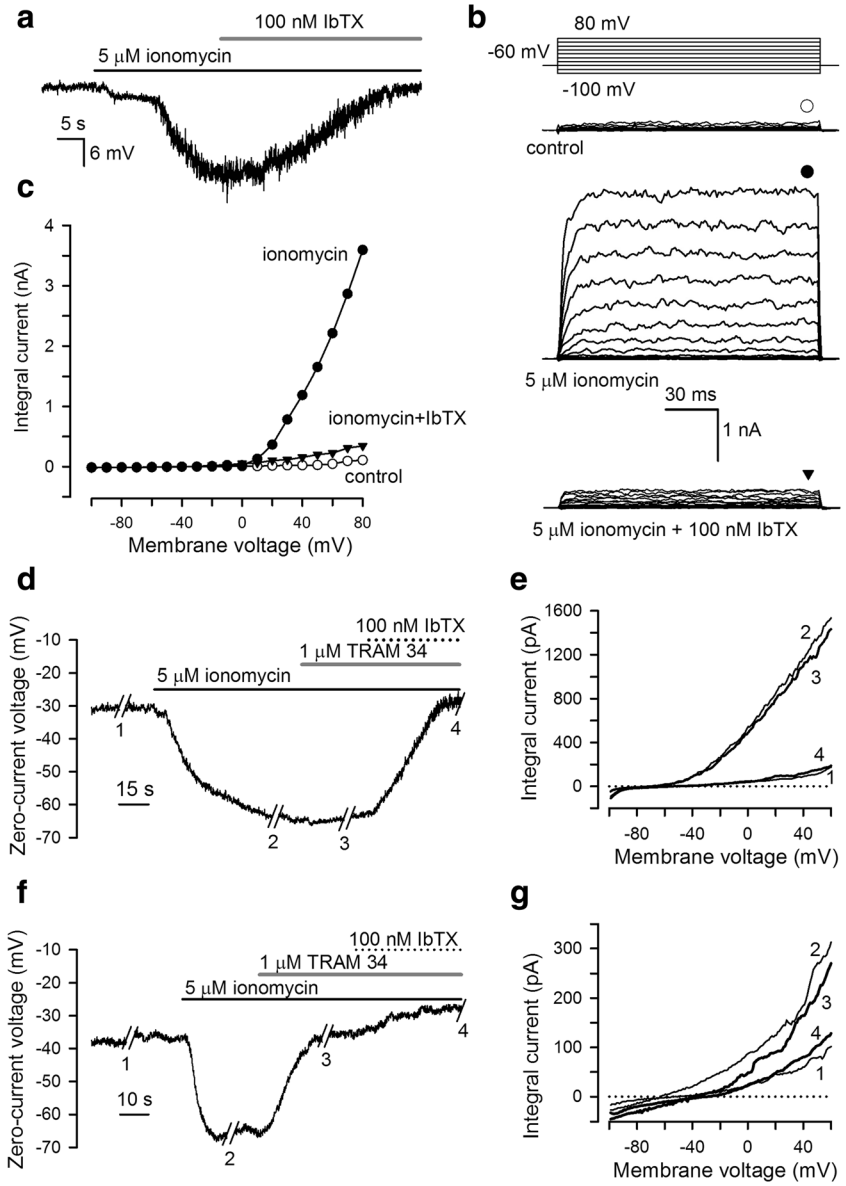

Fig. 3 Ionomycin hyperpolarizes MSC by stimulating Ca^{2+}-gated K^+ channels. **a** Representative (n = 51) recording of membrane voltage in MSC stimulated by 5 μM ionomycin and treated with 100 nM iberiotoxin (IbTX) as indicated by the *horizontal lines above the experimental trace*. **b** Families of integral currents elicited by voltage pulses in the same cell in control, with 5 μM ionomycin in the bath (*middle panel*), and in the presence of 100 nM iberiotoxin (IbTX) as indicated. The *symbols above the current traces* indicate the moments when current values were measured to generate I-V curves shown in (**c**). The assayed cell was held at −60 mV and polarized by 140-ms voltage pulses between −100 and 80 mV. **d** Representative zero-current clamp recording (n = 45) from MSC negligibly sensitive to TRAM-34. A cell was stimulated by 5 μM ionomycin and treated with 1 mM TRAM-34 and 100 nM IbTX as indicated. The recording was interrupted at the moments *1–4* to generate I-V curves by voltage ramp. **e** I-V curves generated in (**d**) at the moments *1–4* indicate that in a given cell, ionomycin stimulated an outwardly rectifying K^+ current that was blocked by IbTX, pointing at $K_{Ca}1.1$ channels to be responsible. **f** Representative recording (n = 6) from a cell sensitive to both TRAM-34 and IbTX. **g** I-V curves generated at the moments *1–4* in (**f**) indicate that both $K_{Ca}1.1$ and $K_{Ca}3.1$ channels were responsible for hyperpolarization of a given cell by ionomycin. The recording conditions were as in Fig. 1

ionomycin stimulated anionic currents, while no evidence for TRPM4 activity in MSCs was obtained. Perhaps, TRPM4-positive cells represent a minor group in a MSC population.

Reportedly, anion currents mediated by Ano1 and Ano2 channels activate slowly and exhibit marked outward rectification at a physiologically moderate level of intracellular Ca^{2+}, while at micromolar Ca^{2+}, those become almost ohmic [12, 46]. Thus, at high intracellular Ca^{2+}, Ano1, and Ano2 channels are poorly distinguishable at the level of integral currents from bestrophin channels, which mediate almost instantly activating and weakly voltage-dependent currents [23, 41]. Yet, at the moment, no subtype-specific blockers of anoctamin and bestrophin channels are available, excluding T16inh-A01 (T16), an inhibitor of Ano1 channels [15]. Because the accurate

control of intracellular Ca^{2+} with ionomycin is hardly possible, we dialyzed MSCs via the patch pipette containing Ca^{2+}-EGTA buffer to maintain 440 nM free Ca^{2+} in CsCl-based intracellular solution. At this concentration of intracellular Ca^{2+}, Ano channels were expected to remain slowly activating, while bestrophin channels should have endowed the plasma membrane with an ohmic conductance.

Overall, we succeeded in sufficiently stable whole-cell (WC) recordings from 48 MSCs held at −60 mV, and in 35 cells (73%), the introduction of 440 nM Ca^{2+} affected insignificantly their resting currents and I-V characteristics that remained nearly linear during dialysis (not shown). This suggested that neither Ca^{2+}-gated anionic channels nor TRPM4 were detectably active in such cells under our recording conditions. Meanwhile, the dialysis greatly increased resting currents in 13 cells (27%) and produced dramatic transformation of their I-V curves (Figs. 4 and 5). Among them, 5 cells reacted to the introduction of 440 nM Ca^{2+} with gradually increasing resting current (Fig. 4a) that was associated with the appearance of slowly activating voltage-gated (VG) currents with strong outward rectification and reversal potential closed to zero voltage (Fig. 4b, c). These Ca^{2+}-dependent currents were significantly suppressed by 100 μM CaCCinh (Fig. 4a, b). Our findings indicated that predominantly, anionic channels were responsible for the slowly activating currents stimulated by intracellular Ca^{2+} at the CsCl/NaCl gradient. Note that these Ca^{2+}-gated anionic currents were insensitive to 10 μM T16 (Fig. 4a, b).

Unexpectedly, we faced the interfering artifact effect of CaCCinh on ion permeability of MSCs: in 23 out of 32 cells treated with CaCCinh, the compound stimulated VG currents at concentrations that were usually sufficient to inhibit Ca^{2+}-gated anion currents (Supplementary Materials, Fig. S2). With 140 mM CsCl in the recording pipette and 140 mM NaCl in the bath, CaCCinh-activated currents reversed between −90 and −80 mV pointing at Cs^+ ions as the main charge carriers. Given this finding and that CaCCinh-activated currents disappeared when 20 mM tetraethylammonium (TEA) was added to the bath (n = 14) (Fig. S2), we inferred that CaCCinh directly or indirectly stimulated VG K^+ channels well permeable

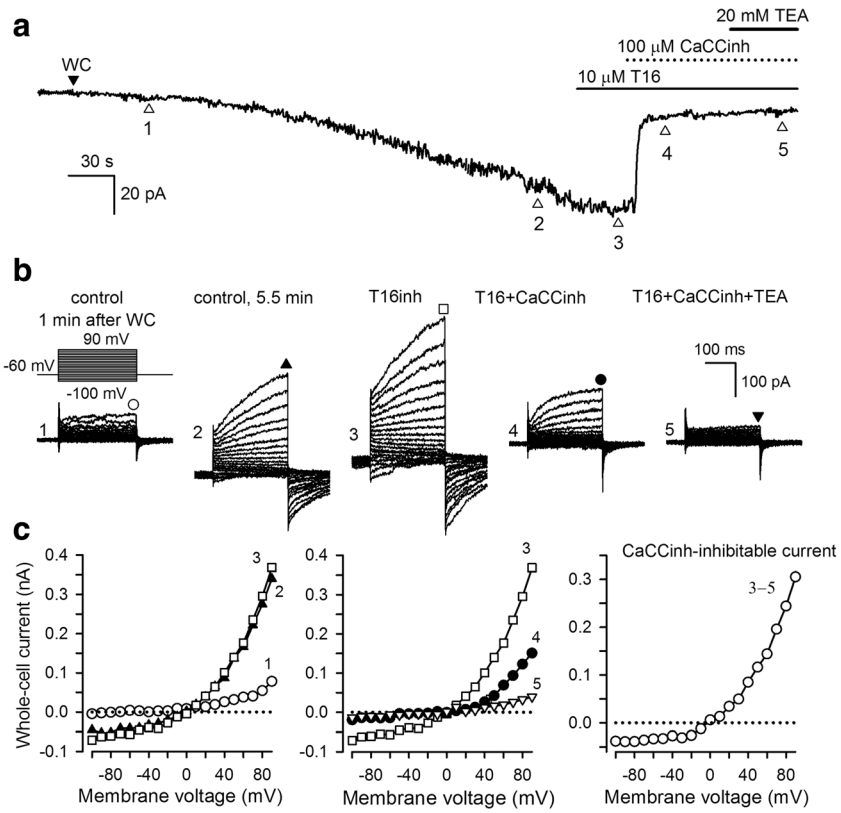

Fig. 4 Slowly activating Ca^{2+}-gated anion currents. **a** Evolution of a *WC* current in a cell held at −60 mV during introduction of 440 nM Ca^{2+}. The Ca^{2+}-dependent current was insensitive to the Ano1 blocker T16 (10 μM) but suppressed by CaCCinh (100 μM), an inhibitor of Ca^{2+}-gated anion channels. At the moments *1–5*, the cell was polarized by 250-ms voltage pulses from −100 to 90 mV to generate I-V curves; the associated current transients were removed from the current trace. The disruption of a cell-attached patch was performed at the moment marked as *WC*. The patch pipette contained 140 mM CsCl and 7.9 mM $CaCl_2$ + 10 mM EGTA (440 nM free Ca^{2+}); 140 mM NaCl was present in the bath. **b** Families of integral currents elicited by voltage pulses and recorded at the corresponding moments *1–5* shown in (**a**). **c** *Left and middle panels*, I-V curves of the integral currents *1–5* shown in (**b**) and measured at the moments indicated by the *symbols above the current traces*. *Right panel*, the I-V curve of the Ca^{2+}-dependent slowly activating current inhibitable with CaCCinh that was calculated as a difference between the *WC* currents recorded at the moments *3* and *5*

to Cs^+ ions. Indeed, although a majority of K^+ channels are negligibly permeable to Cs^+ ions that block many K^+ channel subtypes from both sides of the membrane, Cs^+-permeable K^+ channels also exist (e.g. [26]).

Because TEA inhibited the stimulatory effects of CaCCinh completely (Fig. S2), we calculated a Ca^{2+}-gated anion current as a difference between a WC current recorded when a resting current reached the plateau (Fig. 4a, moment 3) and one measured in the presence of 100 μM CaCCinh +20 mM TEA (Fig. 4a, moment 5). By this approach, CaCCinh-sensitive Ca^{2+}-dependent currents were characterized by I-V curves with strong outward rectification (Fig. 4c, right panel). Kinetically and by the voltage dependence, the responsible Ca^{2+}-gated anionic channels were similar to Ano1/Ano2 channels rather than to bestrophin channels. The insignificant effect of T16 (Fig. 5) argues against a contribution of Ano1, thus implicating Ano2 channels in mediating slowly activating Ca^{2+}-gated anion currents observed in MSCs.

Apart from slowly activating currents (Fig. 4), the introduction of 440 nM Ca^{2+} stimulated activating currents in 13 MSCs almost instantly (Fig. 5). These Ca^{2+}-dependent currents were suppressed by 100 μM CaCCinh (Fig. 5a, b) as well as by 500 μM SITS and 2 mM 9-AC (not shown), suggesting anionic selectivity of responsible Ca^{2+}-gated channels. For the reason mentioned previously, a Ca^{2+}-dependent anion current was evaluated in the presence of 20 mM TEA and determined as a difference between WC currents recorded in control (Fig. 5a, moment 4) and after the addition of 100 μM CaCCinh (Fig. 5a, moment 5). As exemplified by Fig. 5c (right panel), CaCCinh-suppressible currents reversed at nearly zero voltage and exhibited weak outward rectification. The immediate activation kinetics (Fig. 5b) and subtle voltage dependence of these Ca^{2+}-gated anionic currents (Fig. 5b, c, right panel) point at bestrophin channels to be largely responsible for anion flux.

Involvement of $K_{Ca}1.1$ and $K_{Ca}1.1$ channels in transduction of ATP and adenosine

Although the ionomycin treatment of MSCs rendered Ca^{2+}-dependent K^+ and anionic channels active (Figs. 3, 4, and 5), underlying Ca^{2+} signals might be much higher, more lasting, and/or inappropriately localized compared to Ca^{2+} transients elicited by natural agonists. In certain

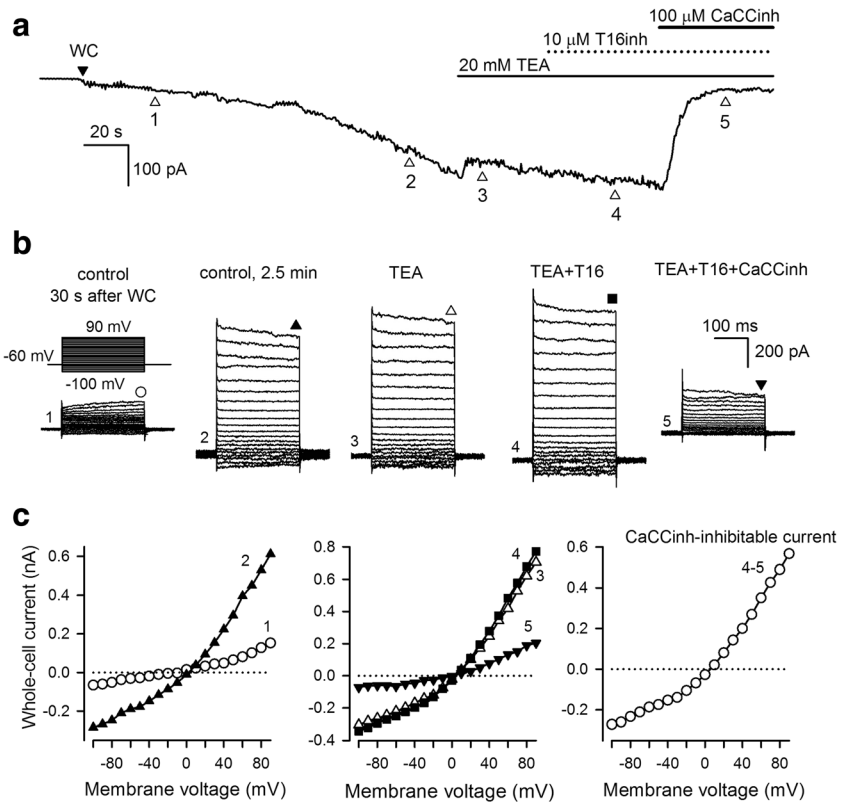

Fig. 5 Instantly activating Ca^{2+}-gated anion currents. **a** Introduction of 440 nM Ca^{2+} stimulated inward current in a cell held at −60 mV and resulted in an increase in membrane conductance as shown in (**b**). At the moments *1–5*, the cell was polarized by 250-ms voltage pulses from −100 to 90 mV to generate I-V curves; the associated current transients were removed from the current trace. **b** The recording conditions were as Fig. 4. **b** Families of integral currents elicited by voltage pulses and recorded at the corresponding moments *1–5* shown in (**a**). **c** *Left and middle panels*, I-V curves of the integral currents 1–5 shown in (**b**) and measured at the moments indicated by the *symbols above the current traces*. *Right panel*, the I-V curve of the Ca^{2+}-dependent, CaCCinh-suppressible, instantly activating current that was calculated as a difference between *WC* currents recorded at the moments *4* and *5*

experiments, we therefore checked whether Ca^{2+}-gated channels could be stimulated by the purinergic agonists ATP and adenosine, both being previously documented by us to mobilize Ca^{2+} in MSCs [35]. To simultaneously monitor intracellular Ca^{2+} and electrophysiological responses to the agonists, MSCs were loaded with Fluo-4. As with oscillating MSCs (Fig. 1), assayed cells were stimulated with 10 μM ATP or 1 μM adenosine; agonist-sensitive MSCs were identified by Ca^{2+} responses, and then those were patched. Overall, we succeeded in conclusive Ca^{2+} imaging/electrophysiological recordings from nine MSCs that remained ATP responsive after patching. These cells were usually clamped at zero current, and recordings of membrane voltage were briefly switched to voltage clamp for generating I-V curves when necessary. In all these cells, a short application of 10 μM ATP elicited marked Ca^{2+} bursts (Fig. 6a, upper panel) that were accompanied by transient membrane hyperpolarization (Fig. 6a, bottom panel, c). By generating I-V curves prior and during ATP application when intracellular Ca^{2+} peaked (Fig. 6b, left panel), it was demonstrated that electrophysiological responses to ATP largely resulted from an increase in outwardly rectifying K^+ conductance (Fig. 6b, right panel). In the presence of 1 μM TRAM-34, voltage responses to 10 μM ATP were nearly twice lower compared to control, although the nucleotide elicited similar Ca^{2+} transients in both cases (Fig. 6a, e). When both TRAM-34 (1 μM) and IbTX (100 nM) were added to the bath, hyperpolarizing ATP responses were completely but reversibly inhibited (Fig. 6a, c). Note that 10 μM ATP insignificantly affected a membrane conductance in the presence of the blockers of $K_{Ca}3.1$ and $K_{Ca}1.1$ channels (Fig. 6d, middle panel). This observation pointed at a negligible contribution of P2X receptors to electrophysiological responses of MSCs to ATP.

Next, we focused on adenosine-sensitive MSCs and obtained overall eight cells with retained capability to respond to adenosine with Ca^{2+} transients after gigaseal formation. In all cases, briefly applied adenosine (1 μM) triggered not only Ca^{2+} bursts but also marked hyperpolarizing voltage responses (Fig. 7a). As for ATP responses (Fig. 6a, b), adenosine stimulated outwardly rectifying currents that reversed at nearly −80 mV (Fig. 7b), the observation implicating Ca^{2+}-gated K^+ channels in mediating adenosine-dependent MSC hyperpolarization. While both Ca^{2+} and voltage responses to 1 μM adenosine were observed in control, this agonist failed to hyperpolarize MSCs with both TRAM-34 and IbTX in the bath, although these blockers could not prevent Ca^{2+} mobilization ($n = 3$) (Fig. 7c). When applied alone, 1 μM TRAM-34 suppressed voltage responses by 40–60% only ($n = 3$) (Fig. 7d, e). It thus appears that $K_{Ca}3.1$ and $K_{Ca}1.1$ channels are functionally co-expressed in ATP- and adenosine-responsive MSCs to couple agonist-dependent Ca^{2+} mobilization to cell hyperpolarization.

Discussion

Several lines of evidence point out that a branched Ca^{2+} signaling system involving multiple signaling pathways operates in MSCs and endows them with high capability to respond to environmental cues [19, 67]. In particular, Kawano and coworkers [31, 32] pioneered in demonstrating spontaneous Ca^{2+} oscillations in MSCs. The oscillatory behavior of intracellular Ca^{2+} in MSCs was associated with paracrine/autocrine release of ATP that stimulated P2Y receptors coupled to phospholipase C (PLC) activation, IP_3 production, and liberation of Ca^{2+} ions from Ca^{2+} store. When enhanced by cyclic ADP-ribose via activation of TRPM2 channels, Ca^{2+} oscillation can stimulate MSC proliferation associated with enhanced ERK1/2 phosphorylation [60]. Reportedly, certain agonists of G-protein-coupled receptors, including adenosine, acetylcholine, ATP, histamine, noradrenaline, and some others, are capable of mobilizing intracellular Ca^{2+} in MSCs [18, 32, 35, 58]. Acetylcholine stimulates MSC migration by involving M1 receptors coupled to the PLC-PKC-ERK1/2 signaling pathway [58]. Functional and molecular evidence indicates that IP_3 receptors serve as dominant Ca^{2+} release channels in MSCs, while a role for ryanodine receptors in Ca^{2+} signaling in these cells remains obscure [32, 35]. In MSCs derived from the human adipose tissue, IP_3 receptors mediate Ca^{2+}-induced Ca^{2+} release, a key intracellular event in adrenergic transduction [35]. Bath Ca^{2+} can influence the proliferation and osteogenic differentiation of MSCs from human bone marrow by stimulating the extracellular Ca^{2+}-sensing receptor coupled to protein kinase C, thus initiating Ras-MAP kinase signaling [2]. Although voltage-gated (VG) Ca^{2+} channels are an attribute of excitable cells, several reports suggest that MSCs also employ these channels [1, 2, 40]. As is the case with apparently all excitable and non-excitable cells, store-operated channels are functional in MSCs as well [32]. The relaxation of Ca^{2+} transients in the MSC cytoplasm involves reticular and plasmalemmal Ca^{2+} ATPases and Na^+/Ca^{2+} exchange [31, 32].

By coupling intracellular Ca^{2+} signals to a change in transmembrane voltage, Ca^{2+}-dependent ion channels may contribute to cellular functions involving transport, receptor, and signaling proteins operating in the plasma membrane. The diverse family of Ca^{2+}-gated channels includes K^+ channels of small ($K_{Ca}2.x$, formerly SK), intermediate ($K_{Ca}3.1$, IK), and large ($K_{Ca}1.1$, BK) conductance [4, 28, 38, 56]; cation channels TRPM4 and TRPM5 [21]; and anion channels [37, 53]. To our knowledge, the activity or expression of any Ca^{2+}-gated anion channel in MSCs has not been demonstrated yet, while functional expression of TRPM4 has been stated in a single report, wherein MSCs from the human adipose tissue were studied [62]. In contrast, multiple reports indicate that Ca^{2+}-gated K^+ channels operate in MSCs from various tissues of different species. In particular, evidence exists that

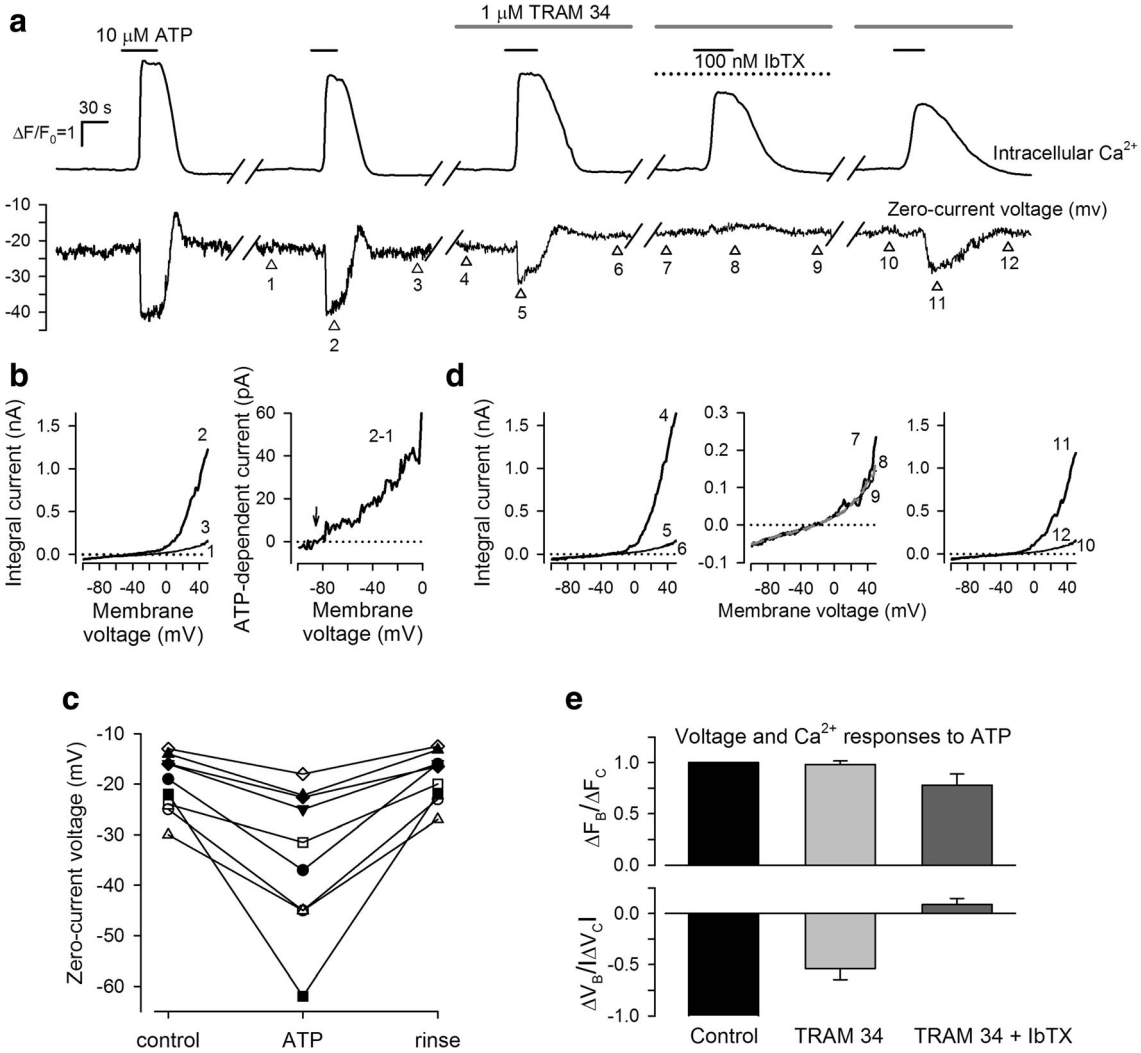

Fig. 6 Voltage and Ca^{2+} responses of MSCs to ATP. **a** Representative concurrent monitoring of intracellular Ca^{2+} (upper panel) and zero-current voltage (*bottom panel*) in MSC loaded with Fluo-4 (n = 9). *Upper panel*, the serial stimulation of a cell with 10 μM ATP elicited large Ca^{2+} transients presented as $\Delta F/F_0$. Bottom panel, voltage responses of the same cell to ATP were partly inhibited by 1 μM TRAM-34 but completely suppressed in the presence of 1 μM TRAM-34 and 100 nM IbTX, suggesting those to be mediated by $K_{Ca}1.1$ and $K_{Ca}3.1$ channels. At the moments *1–12*, I-V curves were generated by voltage ramps (1 mV/ms) from −100 to 80 mV. **b** Being generated in control (*curve 1*), during ATP application (*curve 2*) and after the rinse of ATP and Ca^{2+} relaxation (*curve 3*) (moments *1–3* in (**a**), respectively), the I-V *curves 1–3* pointed out that an ATP-induced rise in intracellular Ca^{2+} was associated with a marked increase in inwardly rectifying conductance (*left panel*). *Right panel*, calculated as a difference between integral currents recorded in the presence of ATP and in control, an ATP-stimulated current reversed below −80 mV (*arrow*). **c** Membrane voltages recorded in nine different cells in control, in the presence of ATP (the first application), and after rinse of the nucleotide. **d** I-V curves generated at the moments *4–12* indicated that outwardly rectifying currents stimulated by ATP were completely and reversibly inhibited by 100 nM IbTX, pointing at $K_{Ca}1.1$ channels to be largely responsible. **e** Summary of Ca^{2+} and voltage responses of MSCs to 10 μM ATP under different conditions. To compare different experiments, each ATP response obtained in the presence of the particular blocker was normalized to a corresponding responses recorded in control. Here, $\Delta F = F_{ATP} - F_0$, where F_0 and F_{ATP} are intensities of cell fluorescence recorded just before ATP application and when intracellular Ca^{2+} peaked, ΔF_C and ΔF_B are Ca^{2+} responses recorded in control and in the presence of the particular blocker; $\Delta V = V_{ATP} - V_0$ where V_0 and V_{ATP} are the membrane voltages recorded before ATP application and when intracellular Ca^{2+} peaked, ΔV_C and ΔV_B are voltage responses recorded in control and in the presence of the particular blocker. The data are presented as a mean ± SD (n = 9). The recording conditions were as in Fig. 1. In line with Student's unpaired t test performed using SigmaPlot (Jandel Scientific), the difference between the control voltage response to ATP and responses recorded in the presence of TRAM-34 and TRAM-34 + IbTX is statistically significant ($P < 0.05$)

$K_{Ca}1.1$ channels are functionally expressed in bone marrow-derived MSCs (BD-MSCs) from the human [24, 32], rabbit [16], and rat [24, 40, 64]. In addition to dominant $K_{Ca}1.1$ channels, rat and rabbit BM-MSCs also express $K_{Ca}3.1$ channels [16, 40, 64]. Mouse BD-MSCs appear to utilize solely $K_{Ca}3.1$ channels. Indeed, among five genes coding for Ca^{2+}-gated K^+ channels, only KCNN4 transcripts were identified in these cells. Yet, no IbTX-blockable currents were

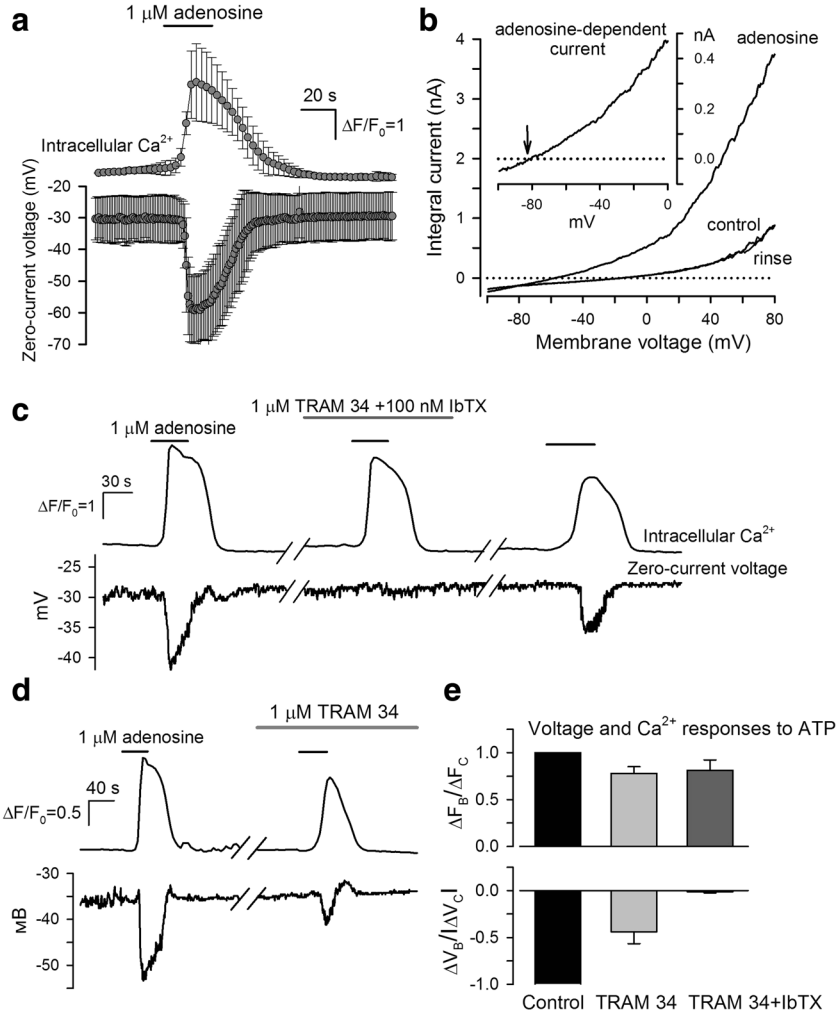

Fig. 7 Voltage and Ca^{2+} responses of MSCs to adenosine. **a** Concurrent monitoring of intracellular Ca^{2+} (*upper panel*) and zero-current voltage (*bottom panel*) in MSC stimulated with 1 μM adenosine. The shown traces were obtained by averaging recordings from eight cells and presented as a mean + SEM **b** Representative I-V curves that were generated in control during adenosine application and after the rinse of the agonist. *Insert*, adenosine-stimualated current, which is calculated as a difference between integral currents recorded in the presence of adenosine and in control, reverses below −80 mV (arrow). **c** Representative concurrent recording of intracellular Ca^{2+} (*upper panel*) and zero-current voltage (*bottom panel*) in MSC stimulated with 1 μM adenosine in control, in the presence of 1 μM TRAM-34 + 100 nM IbTX, and after rinse of the blockers (n = 3). **d** Representative concurrent recording of intracellular Ca^{2+} (*upper panel*) and zero-current voltage (*bottom panel*) in MSC stimulated with 1 μM adenosine in control and in the presence of 1 μM TRAM-34. **e** Summary of Ca^{2+} and voltage responses of MSCs to 1 μM adenosine. Here, ΔF_C, ΔF_B, ΔV_C, and ΔV_B have the same meaning as in Fig. 6e, except for that adenosine responses instead of ATP responses are considered. The data are presented as a mean ± SD (n = 3). The recording conditions were as in Fig. 1. The difference between the control voltage response to ATP and the responses recorded in the presence of TRAM-34 and TRAM-34 + IbTX is statistically significant ($P < 0.05$)

detected in mouse BD-MSCs but solely Ca^{2+}-activated K^+ currents sensitive to clotrimazole, an $K_{Ca}3.1$ channel blocker [59]. $K_{Ca}1.1$ channels also were identified in MSCs from the human umbilical cord vein [43].

Here, we studied MSCs derived from the human adipose tissue (hAD-MSCs). The concurrent monitoring of cytosolic Ca^{2+} and membrane voltage from spontaneously oscillating hAD-MSCs provided the first evidence that intracellular Ca^{2+} signaling in these cells could be coupled to a change in membrane voltage (Fig. 1). Although in this particular case, spontaneous Ca^{2+} bursts elicited cell hyperpolarization by stimulating Ca^{2+}-dependent K^+ channels (Fig. 1), the question remained whether this coupling was universal for all MSCs or specific for the oscillating subpopulation. The expression analysis revealed mRNA transcripts for Ca^{2+}-gated K^+ channels of the $K_{Ca}1.1$ and $K_{Ca}3.1$ types as well as for some other Ca^{2+}-activated channels, including the cationic channels TRPM4 and anionic channels from the anoctamin and bestrophin families (Fig. 2). Theoretically, this set of Ca^{2+}-gated ion channels could allow hAD-MSCs to generate diverse electrophysiological responses, depending on a combination of channel subunits expressed in a given cell and/or

magnitude of Ca^{2+} signals triggered by external stimuli. When we treated hAD-MSCs with the Ca^{2+} ionophore ionomycin, all assayed cells were hyperpolarized by 20–40 mV (Fig. 3). This effect of artificially elevated cytosolic Ca^{2+} was mostly mediated by $K_{Ca}1.1$ channels, which appear to be ubiquitous for hAD-MSCs, although in a small (~12%) cellular subpopulation, $K_{Ca}3.1$ channels also contributed to voltage responses to ionomycin (Fig. 3d, e).

To our knowledge, electrophysiological properties of hAD-MSC were analyzed previously in a single work [1]. Based on functional and molecular data, the authors declared that AD-MSC expresses several families of ion channels, including VG Na^+ channels and Ca^{2+}-activated K^+ channels of all three types. In particular, they detected transcripts for *KCNMA1*, *KCNN3*, and *KCNN4* genes and recorded apamin ($K_{Ca}2.x$ blocker)-, clotrimazole-, and IbTX-sensitive Ca^{2+}-activated K^+ currents in 83, 79, and 31% cellular fractions, respectively. These findings differ from our data in that we detected no Ca^{2+}-activated K^+ currents sensitive to apamin (not shown), although more than 200 AD-MSCs were assayed overall. Consistently, we failed to detect transcripts for the *KCNN1-KCNN3* genes encoding $K_{Ca}2.x$ channels (Fig. 2a). Although at the moment, we cannot reasonably address this inconsistency; somewhat, different protocols of cell isolation and maintenance might result in rather different cellular compositions of AD-MSC populations assayed by us and in the work [1].

When assayed with perforated patch approach and CsCl in the patch pipette, every third cell responded to ionomycin with a marked inward current. This Ca^{2+}-dependent current was negligibly sensitive to the specific TRPM4 blocker 9-phenanthrol (Supplementary Materials, Fig. S1). Thus, despite the detection of TRPM4 transcripts in RNA isolated from hSD-MSC samples (Fig. 2), we failed to get convincing functional evidence for activity of TRPM4 channels. Perhaps, these channels were insufficiently active or not expressed in the vast majority of hSD-MSCs. The introduction of 440 nM Ca^{2+} into hSD-MSCs via the recording pipette stimulated anion currents in some of them (27%), and in all such cells, Ca^{2+}-dependent currents were inhibited by CaCCinh completely. Because subtype-specific antagonists are not available, except for the Ano1 inhibitor T16, it was impossible to judge conclusively on the molecular identity of anionic channels responsible for Ca^{2+}-gated currents. Note, however, that among hAD-MSCs responsive to Ca^{2+} loading, outwardly rectifying slowly activating currents appeared in every third cell as cytosolic Ca^{2+} rose during cell dialysis (Fig. 4). By activation kinetics and voltage dependence (Fig. 4), these currents resembled Ca^{2+}-gated anion currents mediated by Ano1/Ano2 channels [12, 46]. Since T16 exerted negligible effects, Ano2 channels were presumably responsible for these slow anion currents gated by cytosolic Ca^{2+} in hSD-MSCs. In nearly 70% fraction of Ca^{2+}-sensitive cells, elevated cytosolic Ca^{2+} stimulated anion currents that were weakly rectifying and activated by electrical pulses almost instantly (Fig. 5), implicating bestrophin-like channels [41].

In a number of experiments, we analyzed whether Ca^{2+}-gated ion channels identified in hAD-MSCs might couple natural, that is elicited by agonists, Ca^{2+} signals to membrane polarization. The purinergic ligands ATP and adenosine were tested, because previously, we found both to mobilize Ca^{2+} in cells of this type [35]. It turned out that cells responsive, in terms of Ca^{2+} signaling, to 10 μM ATP and 1 μM adenosine were strongly hyperpolarized by both compounds (Figs. 6 and 7). The agonist-dependent hyperpolarization was partly diminished by TRAM-34 (1 μM) and completely disappeared when both TRAM-34 and IbTX (100 nM) were added to the bath (Figs. 6a and 7c). It thus appears that in hAD-MSCs responsive to ATP and adenosine, transduction of these agonists is associated with the generation of Ca^{2+} transients and activation of K^+ channels of the $K_{Ca}1.1$ and $K_{Ca}3.1$ types. It is noteworthy that in some cells, hyperpolarizing voltage responses to the agonists were followed by conspicuous off-responses (Figs. 6a and 7d). This depolarizing phase of voltage responses might be mediated by Ca^{2+}-gated anion channels, deactivation of which during relaxation of Ca^{2+} bursts was presumably delayed due to higher sensitivity to cytosolic Ca^{2+} compared to Ca^{2+}-dependent K^+ channels.

In electrically excitable cells, $K_{Ca}1.1$ channels are usually co-localized with VG Ca^{2+} channels and control both the firing frequency and the action potential repolarization phase, thereby regulating neurotransmission in neurons, contraction in muscles, release of catecholamines in chromaffin cells, and insulin secretion in β cells [38, 63]. The physiological role of $K_{Ca}1.1$ and other Ca^{2+}-gated channels identified in non-excitable cells, including hAD-MSCs, remains poorly understood with few exceptions such as exocrine gland cells. In these cells, the acute regulation of fluid and electrolyte secretion depends on a fine control of $K_{Ca}1.1$ and VG K^+ channels in conjunction with Ca^{2+}-activated Cl^- channels [44–47]. Consistently with the expression of multiple P2Y and P1 purinoreceptors in MSCs of different origin, extracellular ATP and adenosine can modulate certain physiological processes in these cells [52]. Specifically, ATP can serve as adipogenic factor, while adenosine switches off adipogenic differentiation and promotes osteogenesis [10]. Our findings do not provide a clear idea of which cellular functions might depend on plasma membrane hyperpolarization elicited by ATP or adenosine and mediated by $K_{Ca}1.1$ and $K_{Ca}3.1$ channels in in hAD-MSCs. Note that proliferation and migration of diverse cells could be inhibited when activity of $K_{Ca}1.1$ or $K_{Ca}3.1$ channels was suppressed by pharmacological blockage or genetic ablation [8, 20, 27, 36], although the underlying mechanisms were not clarified in most cases. The interesting possibility was proposed by Chandy and co-workers [9], who suggested that sequential activation of VG and Ca^{2+}-activated K^+ channels during mitosis triggers and sustains cell

hyperpolarization in T lymphocytes to facilitate Ca^{2+} entry via CRAC channels, thus stimulating the cell cycle machinery [9]. The somewhat similar mechanism was considered to explain the inhibitory effects of blockers of Ca^{2+}-gated K^+ channels on NO production stimulated by the Ca^{2+} mobilizing agents ATP and histamine in endothelial cells. It was suggested that by regulating Ca^{2+} influx responsible for stimulation of endothelial NO synthase, $K_{Ca}2.x$ and $K_{Ca}3.1$ channel-mediated hyperpolarization represents a critical early event in agonist-evoked NO production [54]. Interestingly, NO has been reported as a MSC-derived modulator of T-cell proliferation in the mouse at least [51]. The similar hyperpolarization-dependent regulation of Ca^{2+} entry may take place in hAD-MSCs as a part of intracellular signaling stimulated by ATP and adenosine. Human MSCs secrete important regulatory molecules such as cytokines, growth factors, and hormones as well as microvesicles and exosomes containing not only peptides but also microRNA [55]. The non-constitutive Ca^{2+}-dependent exocytosis in MSCs might vary with activity of $K_{Ca}1.1$ and $K_{Ca}3.1$ channels, which should modulate Ca^{2+} influx. Hopefully, further experiments will allow for verifying the physiological role of $K_{Ca}1.1$ and $K_{Ca}3.1$ channels in hAD-MSC functioning.

Acknowledgements This work was supported by the Russian Science Foundation (grants 14-14-00687) and the Russian Foundation for Basic Research (grant 14-04-01711a).

References

1. Bai X, Ma J, Pan Z et al (2007) Electrophysiological properties of human adipose tissue-derived stem cells. Am J Physiol Cell Physiol 293:1539–1550
2. Barradas AM, Fernandes HA, Groen N et al (2012) A calcium-induced signaling cascade leading to osteogenic differentiation of human bone marrow-derived mesenchymal stromal cells. Biomaterials 33:3205–3215
3. Becchetti A (2011) Ion channels and transporters in cancer. 1. Ion channels and cell proliferation in cancer. Am J Physiol Cell Physiol 301:255–265
4. Bertuccio CA, Devor DC (2015) Intermediate conductance, Ca^{2+}-activated K^+ channels: a novel target for chronic renal diseases. Front Biol 10:52–60
5. Blackiston DJ, McLaughlin KA, Levin M (2009) Bioelectric controls of cell proliferation ion channels, membrane voltage and the cell cycle. Cell Cycle 8:3527–3536
6. Campagnoli C, Roberts IA, Kumar S et al (2001) Identification of mesenchymal stem/progenitor cells in human first-trimester fetal blood, liver, and bone marrow. Blood 98:2396–2402
7. Capiod T (2011) Cell proliferation, calcium influx and calcium channels. Biochimie 93:2075–2079
8. Catacuzzeno L, Caramia M, Sforna L et al (2015) Reconciling the discrepancies on the involvement of large-conductance Ca^{2+}-activated K channels in glioblastoma cell migration. Front Cell Neurosci 9:152
9. Chandy KG, Wulff H, Beeton C et al (2004) K^+ channels as targets for specific immunomodulation. Trends Pharmacol Sci 25:280–289
10. Ciciarello M, Zini R, Rossi L, Salvestrini V, Ferrari D, Manfredini R, Lemoli RM (2013) Extracellular purines promote the differentiation of human bone marrow-derived mesenchymal stem cells to the osteogenic and adipogenic lineages. Stem Cells Dev 22(7):1097–1111
11. Cheng H, Feng JM, Figueiredo ML et al (2010) Transient receptor potential melastatin type 7 channel is critical for the survival of bone marrow derived mesenchymal stem cells. Stem Cells Dev 19:1393–1403
12. Cherkashin AP, Kolesnikova AS, Tarasov MV et al (2016) Expression of calcium-activated chloride channels Ano1 and Ano2 in mouse taste cells. Pflugers Arch 468:305–319
13. Cidad P, Jimenez-Perez L, Garcia-Arribas D et al (2012) Kv1.3 channels can modulate cell proliferation during phenotypic switch by an ion-flux independent mechanism. Arterioscler Thromb Vasc Biol 32:1299–1307
14. Clapham DE (2007) Calcium signaling. Cell 131:1047–1058
15. De La Fuente R, Namkung W, Mills A et al (2008) Small-molecule screen identifies inhibitors of a human intestinal calcium-activated chloride channel. Mol Pharmacol 73:758–768
16. Deng XL, Sun HY, Lau CP, Li GR (2006) Properties of ion channels in rabbit mesenchymal stem cells from bone marrow. Biochem Biophys Res Commun 348:301–309
17. Dominici M, Le Blanc K, Mueller I et al (2006) Minimal criteria for defining multipotent mesenchymal stromal cells. The International Society for Cellular Therapy position statement, Cytotherapy 8: 315–317
18. Ferrari D, Gulinelli S, Salvestrini V et al (2011) Purinergic stimulation of human mesenchymal stem cells potentiates their chemotactic response to CXCL12 and increases the homing capacity and production of proinflammatory cytokines. Exp Hematol 39:360–374
19. Forostyak O, Forostyak S, Kortus S et al (2016) Physiology of Ca^{2+} signalling in stem cells of different origins and differentiation stages. Cell Calcium 59:57–66
20. Grgic I, Eichler P, Heinau et al. (2005) Selective blockade of the intermediate-conductance Ca^{2+}-activated K^+ channel suppresses proliferation of microvascular and macrovascular endothelial cells and angiogenesis in vivo. Arterioscler Thromb Vasc Biol 25:704–709
21. Guinamard R, Salle L, Simard C (2011) The non-selective monovalent cationic channels TRPM4 and TRPM5. In: Islam MS (ed) Transient receptor potential channels. Springer, Netherlands, pp. 147–171
22. Guinamard, R., Hof, T. and Del Negro, C. A. (2014) The TRPM4 channel inhibitor 9-phenanthrol. Br J Pharmacol 1600–1613
23. Hartzell HC, Qu Z, Yu K, Xiao Q, Chien LT (2008) Molecular physiology of bestrophins: multifunctional membrane proteins linked to best disease and other retinopathies. Physiol Rev 88: 639–672
24. Heubach JF, Graf EM, Leutheuser J et al (2004) Electrophysiological properties of human mesenchymal stem cells. J Physiol Lond 554:659–672
25. Im GI, Shin YW, Lee KB (2005) Do adipose tissue-derived mesenchymal stem cells have the same osteogenic and chondrogenic potential as bone marrow-derived cells? Osteoarthr Cartil 13:845–853
26. Ishii H, Nakajo K, Yanagawa Y, Kubo Y (2010) Identification and characterization of Cs^+ -permeable K^+ channel current in mouse cerebellar Purkinje cells in lobules 9 and 10 evoked by molecular layer stimulation. Eur J Neurosci 32:736–748
27. Jackson WF (2005) Potassium channels and proliferation of vascular smooth muscle cells. Circ Res 97:1211–1212
28. Jensen BS, Hertz M, Christophersen P, Madsen LS (2002) The Ca^{2+}-activated K^+ channel of intermediate conductance: a possible target for immune suppression. Expert Opin Ther Targets 6:623–636
29. Jia X, Yang J, Song W (2013) Involvement of large conductance Ca^{2+}-activated K^+ channel in laminar shear stress-induced inhibition of vascular smooth muscle cell proliferation. Pflugers Arch 465:221–232

30. Kalinina NI, Sysoeva VY, Rubina KA et al (2011) Mesenchymal stem cells in tissue growth and repair. Acta Nat 3:30–37
31. Kawano S, Otsu K, Kuruma A et al (2006) ATP autocrine/paracrine signaling induces calcium oscillations and NFAT activation in human mesenchymal stem cells. Cell Calcium 39:313–324
32. Kawano S, Shoji S, Ichiose S et al (2002) Characterization of Ca^{2+} signaling pathways in human mesenchymal stem cells. Cell Calcium 32:165–174
33. Kawashima N (2012) Characterisation of dental pulp stem cells: a new horizon for tissue regeneration? Arch Oral Biol 57:1439–1458
34. Kolesnikov SS, Margolskee RF (1998) Extracellular K^+ activates a K^+- and H^+-permeable conductance in frog taste receptor cells. J Physiol Lond 1:415–432
35. Kotova PD, Sysoeva VY, Rogachevskaja OA et al (2014) Functional expression of adrenoreceptors in mesenchymal stromal cells derived from the human adipose tissue. Biochim Biophys Acta 1843:1899–1908
36. Kraft R, Krause P, Jung S et al (2003) BK channel openers inhibit migration of human glioma cells. Pflugers Arch 446:248–255
37. Kunzelmann K (2015) TMEM16, LRRC8A, bestrophin: chloride channels controlled by Ca^{2+} and cell volume. Trends Biochem Sci 40:535–543
38. Latorre R, Gonzalez C, Rojas P (2013) Signal transduction-dependent channels. In: Pfaff DW (ed) Neuroscience in the 21st century, Springer Science+Business Media, LLC, pp 81–107
39. Le Blanc K, Mougiakakos D (2012) Multipotent mesenchymal stromal cells and the innate immune system. Nat Rev Immunol 12:383–396
40. Li GR, Deng XL, Sun H et al (2006) Ion channels in mesenchymal stem cells from rat bone marrow. Stem Cells 24:1519–1528
41. Milenkovic VM, Soria RB, Aldehni F, Schreiber R, Kunzelmann K (2009) Functional assembly and purinergic activation of bestrophins. Pflugers Arch 458:431–441
42. Nelson P, Ngoc Tran TD, Zhang H et al (2013) Transient receptor potential melastatin 4 channel controls calcium signals and dental follicle stem cell differentiation. Stem Cells 31:167–177
43. Park KS, Jung KH, Kim SH et al (2007) Functional expression of ion channels in mesenchymal stem cells derived from umbilical cord vein. Stem Cells 25:2044–2052
44. Pifferi S, Dibattista M, Menini A (2009) TMEM16B induces chloride currents activated by calcium in mammalian cells. Pflugers Arch 458:1023–1038
45. Pillozzi S, Becchetti A (2012) Ion channels in hematopoietic and mesenchymal stem cells. Stem Cells Int 2012. Doi:10.1155/2012/217910
46. Petersen OH, Maruyama Y (1984) Calcium-activated potassium channels and their role in secretion. Nature 307:693–696
47. Petersen OH (1992) Stimulus-secretion coupling: cytoplasmic calcium signals and the control of ion channels in exocrine acinar cells. J Physiol 448:1–51
48. Resende RR, Andrade LM, Oliveira AG et al (2013) Nucleoplasmic calcium signaling and cell proliferation: calcium signaling in the nucleus. Cell Commun Signal 11:14
49. Rizzuto R, Pozzan T (2006) Microdomains of intracellular Ca^{2+}: molecular determinants and functional consequences. Physiol Rev 86:369–408
50. Salkoff L, Butler A, Ferreira G et al (2006) High-conductance potassium channels of the SLO family. Nat Rev Neurosci 7:921–931
51. Sato K, Ozaki K, Oh I, Meguro A, Hatanaka K, Nagai T, Muroi K, Ozawa K (2007) Nitric oxide plays a critical role in suppression of T-cell proliferation by mesenchymal stem cells. Blood 109:228–234
52. Scarfì S (2014) Purinergic receptors and nucleotide processing ectoenzymes: their roles in regulating mesenchymal stem cell functions. World J. Stem Cells 6:153–162
53. Scudieri P, Sondo E, Ferrera L et al (2012) The anoctamin family: TMEM16A and TMEM16B as calcium-activated chloride channels. Exp Physiol 97:177–183
54. Sheng J-Z, Braun AP (2007) Small- and intermediate-conductance Ca^{2+}-activated K^+ channels directly control agonist-evoked nitric oxide synthesis in human vascular endothelial cells. Am J Physiol Cell Physiol 293:C458–C467
55. Spees JL, Lee RH, Gregory CA (2016) Mechanisms of mesenchymal stem/stromal cell function. Stem Cell Res Ther 7:125
56. Stocker M (2004) Ca^{2+}-activated K^+ channels: molecular determinants and function of the SK family. Nat Rev Neurosci 5:758–770
57. Sundelacruz S, Levin M, Kaplan DL (2009) Role of membrane potential in the regulation of cell proliferation and differentiation. Stem Cell Rev 5:231–246
58. Tang JM, Yuan J, Li Q et al (2012) Acetylcholine induces mesenchymal stem cell migration via Ca^{2+}/PKC/ERK1/2 signal pathway. J Cell Biochem 113:2704–2713
59. Tao R, Lau CP, Tse HF, Li GR (2007) Functional ion channels in mouse bone marrow mesenchymal stem cells. Am J Physiol Cell Physiol 293:1561–1567
60. Tao R, Sun HY, Lau CP et al (2011) Cyclic ADP ribose is a novel regulator of intracellular Ca^{2+} oscillations in human bone marrow mesenchymal stem cells. J Cell Mol Med 15:2684–2696
61. Toro L, Li M, Zhang Z et al (2014) MaxiK channel and cell signaling. Pflugers Arch 466:875–886
62. Tran TD, Zolochevska O, Figueiredo ML et al (2014) Histamine-induced Ca^{2+} signalling is mediated by TRPM4 channels in human adipose-derived stem cells. Biochem J 463:123–134
63. Vandael DH, Marcantoni A, Mahapatra S et al (2010) $Ca_v1.3$ and BK channels for timing and regulating cell firing. Mol Neurobiol 42:185–198
64. Wang SP, Wang JA, Luo RH et al (2008) Potassium channel currents in rat mesenchymal stem cells and their possible roles in cell proliferation. Clin Exp Pharmacol Physiol 35:1077–1084
65. Wei AD, Gutman GA, Aldrich R et al (2005) International Union of Pharmacology. LII. Nomenclature and molecular relationships of calcium activated potassium channels. Pharmacol Rev 57:463–472
66. Wei J-F, Wei L, Zhou X et al (2008) Formation of Kv2.1-FAK complex as a mechanism of FAK activation, cell polarization and enhanced motility. J Cell Physiol 217:544–557
67. Ye B (2010) Ca^{2+} oscillations and its transporters in mesenchymal stem cells. Physiol Res 59:323–329